Structural information and (hyper)graph matching for MRI piglet brain extraction

A. Durandeau[1], J.-B. Fasquel[1], I. Bloch[2], E Mazerand[3], P Menei[3,4], C. Montero-Menei[3], M. Dinomais[1,5]

1 LARIS EA7315, Université d'Angers, France
2 LTCI, Télécom ParisTech, Université de Paris-Saclay, France
3 CRCINA, INSERM, Nantes University, Université d'Angers, France
4 Departement of neurosurgery, Centre Hospitalier Universitaire d'Angers, France
5 Department of physical and rehabilitation medicine, Centre Hospitalier Universitaire d'Angers, France

Keywords: Structural information, graph matching, hypergraph matching, brain imaging, MRI, piglet

Abstract

In the context of the study of the maturation process of the infant brain, this paper focuses on postnatal piglet brain, whose structure is similar to the one of an infant. Due to the small size of the piglet brain and the abundance of surrounding fat and muscles, the automatic brain extraction using correctely initialized deformable models is tedious, and the standard approach used for human brain does not apply. The paper proposes an original brain extraction method based on a deformable model, whose initialization is guided by *a priori* known relationships between some anatomical structures of the head. This concerns a structural model related to *a priori* known inclusion and photometric relationships between eyes, nose and other internal head entities (fat and muscles). This *a priori* structural information also involves the relative position of both eyes and nose, assumed to be an anatomical invariant similar to a triangle. Using this structural model, our proposal detects both eyes and nose, from which one deduces the brain center, for finally initializing deformable models. Anatomical structures are retrieved by matching observed relationships with those embedded in the *a priori* structural model. This involves graph and hypergraph matching, where hypergraph matching concerns relative position of eyes and nose (ternary constraint related to these 3 entities). The method has been implemented and preliminary experiments have been performed on a set of 6 piglets, to evaluate the accuracy of the brain center localization, the one of the final brain extraction using deformable models. The brain center is correctly localized with a mean error of 1.7 mm, underlying the relevance of the approach. The mean similarity index has been measured to be of 0.85 (with a standard deviation of 0.04). More generally, this work illustrates the potential of considering high level *a priori* known relationships, related to anatomical invariants, managed using graph and hypergraph matching.

1 Introduction

Piglets are increasingly used as an animal model for human infants due to the fact that their brain structure and function are similar to the ones of infants [1]. Therefore, studying piglet brain helps to better understand the maturation process of infant brains, and to anticipate future neuro-developmental disorders [2]. Magnetic resonance imaging (MRI) is a useful image modality for monitoring this maturation process [1, 3]. A major difficulty concerns the automated segmentation of brain structure from MR images. Although many works have been achieved for human infant brains [3], few has been done for piglets. We can mention a recent work which focused on the building of piglet brain atlas [1], in order to automate the segmentation of internal brain structures using an altas-based approach, as often considered for human brains. A difficulty concerns the automated segmentation of the entire brain, being a crucial preliminary step before segmenting internal structures. For instance, in [1], the entire brain mask is manually drawn, this being really time consuming, and unappropriate for building of large databases of segmented piglet brains. Due to the abundance of muscle and fat in the piglet's head [1], techniques considered for human brain cannot be applied. For instance, we can mention the widely used BET algorithm (Brain Extraction Tool) [4, 5]. This algorithm uses deformable models initialized by a sphere centered on the center of mass of the entire human head. This is appropriate for human head due to the surrounding thin skull allowing a relevant estimate of the brain center of mass, this being difficult for piglet, due to the previously mentioned abundance of muscle and fat.

This work aims at overcoming this limitation, by initializing deformable models using the relative position of piglet brain with respect to eyes and nose, appearing as dark anatomical structures that are assumed to be easy to segment. This proposal constitutes the main contribution of this work, providing an entire fully automated brain segmentation technique, allowing to then perform the segmentation of internal brain structures [1]. The proposed approach is based on the *a priori* knowledge of the photometric, topological and spatial structure of piglet head. In our case, we consider another approach based on a qualitative *a priori* knowledge related to the perception of

the structure of the head in the image (spatial relationships as well as photometric and inclusion ones). For instance, eyes and nose appear darker than any other structure (photometric relationships), and belong to the piglet head (inclusion relationships). The nose and both eyes represent three points, that are spatially similar to a triangle (spatial relationships). Such a kind of approach facilitates the declaration of the model (i.e. *a priori* relationships) used for interpreting the scene content [6, 7, 8, 9, 10, 11, 12]. This overcomes the limitation of techniques based on deep learning (see [13] for a recent review of such a technique for brain imaging) that is well known to be efficient but requires a really large learning database, often difficult to acquire and to annotate. Such a structural approach has already shown its potential for medical image analysis, where, for instance, the *a priori* knowledge of spatial and photometric relationships between anatomical and pathological structures can help in guiding interpretation [8, 9, 10, 11, 12]. A major difficulty is to fill the gap between the high level structural knowledge and low level image properties (i.e. at voxels level) [6, 7]. Structural information is often expressed as a graph of relationships between structures and image interpretation is regarded as a graph matching problem. This graph matching can be seen as a set of binary constraints to be verified, regarding inclusion and photometric relationships in our case. In this work, we also consider ternary constraints that we propose to express as a hypergraph matching problem [14, 15]. In our case, hypergraph matching is required to recover the three structures (both eyes and the nose) that are declared to be similar, in terms of spatial relationships, to an isosceles triangle (ternary constraint). The localization of these three structures allows to estimate the center of mass of the brain, assuming that its relative position (with respect to eyes and nose) is stable over piglets. Deformable models, initialized by a sphere centered at this center of mass, are finally used, as for the human brain, to recover the entire piglet brain.

Section 2 presents the proposed approach, including an overview of the entire processing sequence. Preliminary experiments are presented in Section 3, before concluding in Section 4.

2 Method

2.1 Overview

The proposed approach depicts severals steps, summarized by Figure 1. It is based on *a priori* known relationships, detailed in Section 2.2. From the initial MR image (Figure 1-A), nose and eyes candidates are first recovered (Figure 1-B, detailed in Section 2.3) using *a priori* inclusion and photometric relationships, with an approach that is similar to one recently proposed [7]. Step C, being formulated as a hypergraph matching problem [14, 15], aims at recovering the nose and both eyes, this being detailed in Section 2.4. The brain is finally segmented using a deformable model initialized by a sphere placed at brain center, this center being estimated relatively to previous localized nose and eyes (Figure 1-D, detailed in Section 2.5).

2.2 A priori structural model

The *a priori* structural model is based on relationships between four structures of the piglet head: nose, both eyes and remaining internal head structures (mainly muscles and fat). We consider that the image I is composed of a set of regions $R(u), u \in N$, with $N = \{\text{MF, Leye, Reye, Nose}\}$ (`MF`, `Leye` and `Reye` respectively stands for "muscles and fat", "left eye" and "right eye"). Relationships are represented by three graphs, embedding inclusion relationships ($G_{T,m} = (N, A_{T,m})$ graph, where the subscript "T" stands for topology), photometric relationships ($G_{P,m} = (N, A_{P,m})$ graph, where the subscript "P" stands for photometry) and spatial relationships ($G_{S,m} = (N_S, A_{S,m}, \mu_m)$ graph, where the subscript "S" stands for spatial). Spatial relationships concern the relative position of structures. For $G_{S,m}$, the set of nodes is $N_S = N \setminus \{\texttt{MF}\}$, because the considered spatial relationships do not involve muscles nor fat (see Figure 1-C). The subscript m stands for model. These relationships are related to a qualitative description of the scene content, that could be expressed by notions such as "A is included in B" (inclusion relationships), "A is brighter than B" (photometric relationships), "A is similarly bright as B" (photometric relationships), "the distance between A and B is about 50 mm" (spatial relationships and semi-qualitative description).

Concerning $G_{T,m} = (N, A_{T,m})$, edges (A_T set) correspond to inclusion relationships [6, 7], defined by (see Figure 1-B):

$$i \xrightarrow{T} j \Leftrightarrow R(i) \subsetneq R(j). \tag{1}$$

Concerning $G_P = (S, A_{P,m})$, edges ($A_{P,m}$ set) denote order relations between mean intensities of regions [6, 7], and are defined by (see Figure 1-B):

$$i \xrightarrow{P} j \Leftrightarrow \bar{R}(i) \leq \bar{R}(j), \tag{2}$$

$$i \xleftrightarrow{P} j \Leftrightarrow \bar{R}(i) \simeq \bar{R}(j), \tag{3}$$

where $\bar{R}(i)$ is the mean intensity value of region $R(i)$:

$$\bar{R}(i) = \sum_{p \in R(i)} \frac{I(p)}{|R(i)|} \tag{4}$$

Concerning $G_{S,m} = (N_S, A_{S,m}, \mu_m)$, edges ($A_{S,m}$ set) correspond to distances between regions, related to edges attributes defined by the μ_m function:

$$\forall (i,j) \in A_S, \mu_m(i,j) = d(R(i), R(j)). \tag{5}$$

In our case, the considered distance is the euclidean distance between region barycenters.

Both $G_{T,m}$ and $G_{P,m}$ graphs are only used to detect nose and eyes candidates, merged into a single image region (Figure 1-B, detailed in next Section 2.3). The $G_{S,m}$ graph is then used to retrieve each eye and the nose from this region (detailed in Section 2.4).

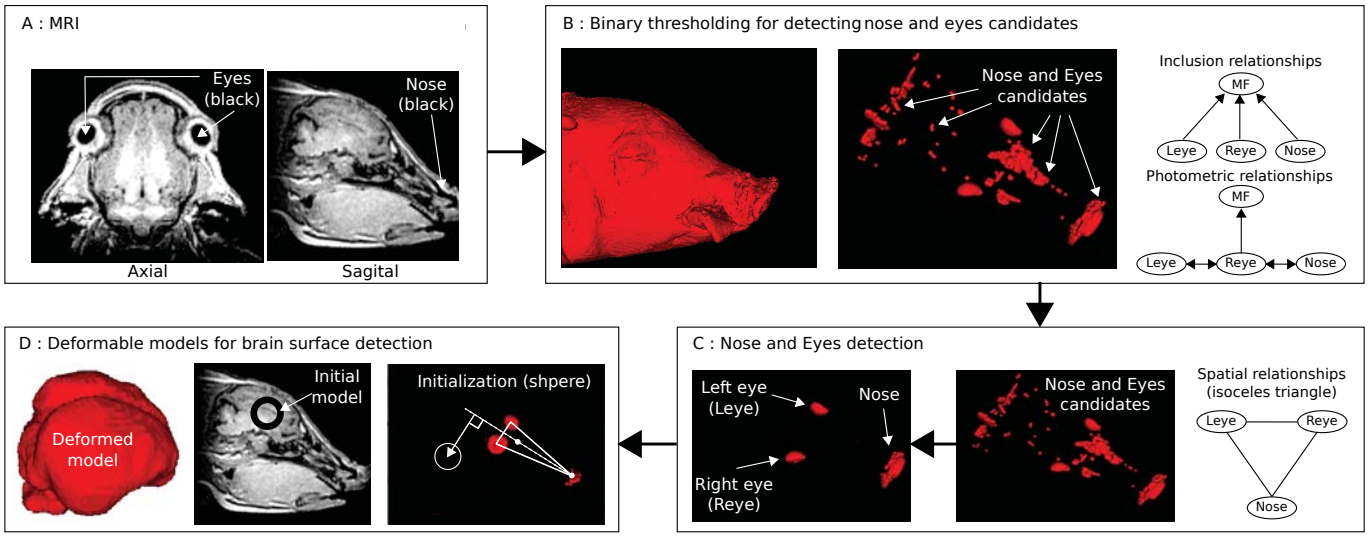

Figure 1. Overview of the proposed brain segmentation approach, based on *a priori* known relationships (inclusion, photometric and spatial relationships) between different entities: `MF` (standing for muscules and fat), `Leye` (left eye), `Reye` (right eye) and `Nose`. From the MR image (A), one detects nose and eyes candidates (B), knowing that they are included in `MF` (inclusion relationships) and darker than `MF` (photometric relationships, where '$\leftrightarrow$' declares similar intensities). The C step recognizes the nose and both eyes, by analyzing the relative position of candidates. The D step aims at recovering brain boundaries using deformable models initialized by a sphere placed at the brain center, being estimated from the position of the nose and both eyes.

2.3 Nose and eyes candidates detection

This step corresponds to Figure 1-B. The processing line for this step starts by segmenting the entire head of the piglet, mainly based on a binary thresholding, leading to the `MF` entity. Nose and eyes candidates are then searched using a binary thresholding constrained to the region of interest defined by this head region, according to inclusion relationships declaring that targets (i.e. eyes and nose) belong to head ($G_{T,m}$). The region of interest is automatically computed from the *a priori* knowledge (inclusion relationships) and the contextual knowledge (fact that the region $R(\texttt{MF})$ is identified), as detailed in [7]. As considered in [7], a binary thresholding is considered because, according to *a priori* photometric relationships, only two classes C_1 and C_2 of photometrically different structures are assumed to belong to the region of interest (declared in $G_P = (S, A_{P,m})$): $C_1 = \{\texttt{MF}\}$ (bright) and $C_2 = \{\texttt{Leye}, \texttt{Reye}, \texttt{Nose}\}$ (black). This identification is performed by a simple exact graph matching approach, based on photometric information only [7]. It involves the photometric graph $G_{P,r} = (M, B_{P,r})$ ("r" stands for real image), built from measured intensities of both classes ($M = \{C_1, C_2\}$). This graph is then matched with the model graph $G_{P,m}$, to automatically identify that C_2 corresponds to the nose and both eyes.

Even if only basic image processing operators are involved, this approach aims at facilitating the guidance of operators (i.e. ROI, number of classes for thresholding) and the identification of outputs (i.e. nose and eyes candidates), based on a simple preliminary declaration of observed relationships.

2.4 Nose and eyes detection

This step corresponds to Figure 1-C. The purpose is to find the three regions corresponding to $N_S = \{\texttt{Leye}, \texttt{Reye}, \texttt{Nose}\}$, that are initially merged, together with artefacts, within the region corresponding to the previously mentionned C_2 entity. We propose to exploit *a priori* known spatial relationships, corresponding to the undirected graph $G_{S,m}$. For this, one first builds the graph associated with the real image: $G_{S,r} = (M, B_{S,r}, \mu_r)$, where "r" stands for real image. The purpose is to find the best matching g between the sets N_S and M. Because $M \neq N_S$, one faces an inexact graph matching problem [6]. In our case, we have the following constraint on g: $\forall i \in N_S, \exists! j \in M \mid g(i) = j$ and $\forall (i,j) \in N_S^2, i \neq j \Leftrightarrow g(i) \neq g(j)$. By considering an association matrix X ($X_{i,j} = 1 \Leftrightarrow j = g(i)$), we can define the set P of all possible matchings verifying these constraints [14]:

$$P = \{X \in \{0,1\}^{|N_S| \times |M|} \mid \sum_{i=1}^{|N_S|} X_{ij} \leq 1, \sum_{j=1}^{|M|} X_{ij} = 1\} \quad (6)$$

In our case, one can exploit some inter-edge properties such as the symmetry of both eyes. This means the matching must be expressed so that it can support such ternary contraints (i.e. constraints regarding simultaneously the three nodes and edges of the model). This can be formulated as a hypergraph matching problem [14, 15], corresponding to hypergraphs $\bar{G}_{S,m} = (N_S, \bar{A}_{S,m})$ and $\bar{G}_{S,r} = (N_S, \bar{A}_{S,r})$. In our case, a hyperedge is defined by a set of three nodes. The set of hyperedges $\bar{A}_{S,m}$ contains a single element: $\bar{A}_{S,m} = \{(\texttt{Leye}, \texttt{Reye}, \texttt{Nose})\}$. The set of hyperedges $\bar{A}_{S,r}$ contains all possible sets of three

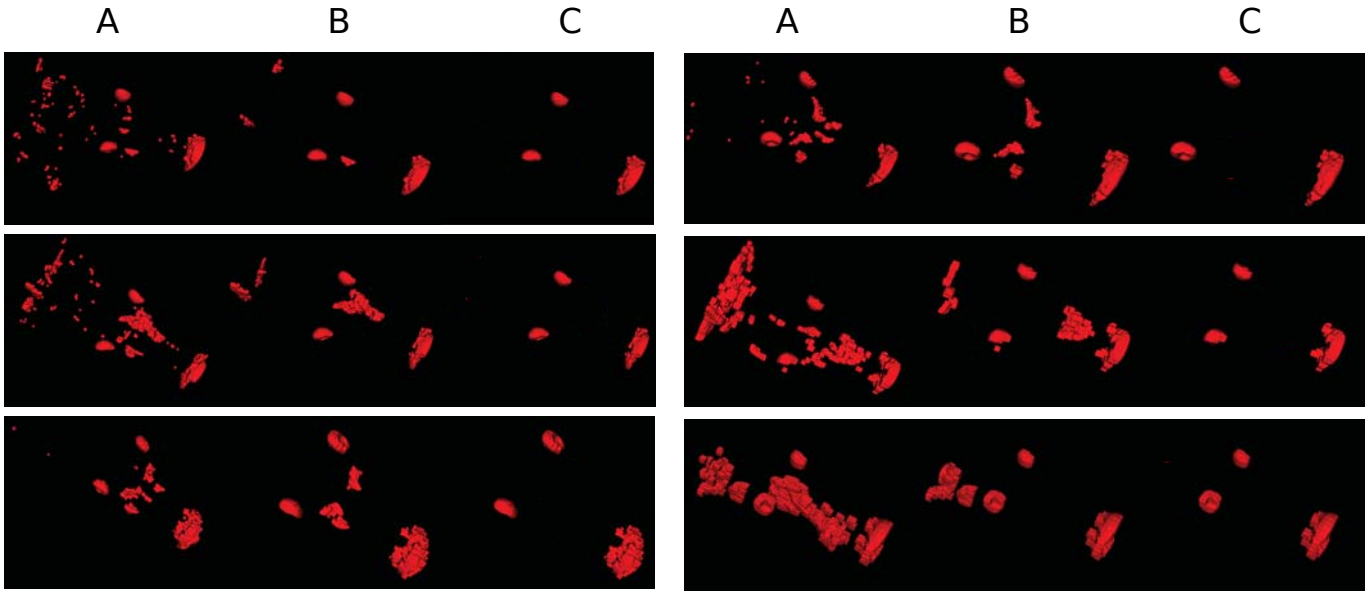

Figure 2. Matching results over the 6 piglets. A: After thresholding. B: After filtering (removal of small connected components). C: Recovered eyes and nose, resulting from the hypergraph matching with the model.

elements of M: $\bar{A}_{S,r} = \{(i,j,k) \in M^3\}$.

As in [14], we consider a tensor formulation of hypergraph matching, using a 6D supersymmetric tensor H, used to evaluate a score S of a matching $X \in P$:

$$S(X) = \sum_{i_1,i_2,j_1,j_2,k_1,k_2} H_{i_1,i_2,j_1,j_2,k_1,k_2} X_{i_1,i_2} X_{j_1,j_2} X_{k_1,k_2} \tag{7}$$

The product $X_{i_1,i_2}X_{j_1,j_2}X_{k_1,k_2}$ is equal to 1 if and only if points $(i_1,j_1,k_1) \in \bar{A}_{S,m}$ are, respectively, matched to the points $(i_2,j_2,k_2) \in \bar{A}_{S,r}$. In this case, it will add $H_{i_1,i_2,j_1,j_2,k_1,k_2}$ to the total score function and 0 otherwise. Note that the tensor H is supersymmetric because invariant under permutations in (i_1,j_1,k_1) or (i_2,j_2,k_2). H represents a similarity measure between matched triangles:

$$\forall (i_1,j_1,k_1) \in \bar{A}_{S,m}, (i_2,j_2,k_2) \in \bar{A}_{S,r}, \\ H_{i_1,i_2,j_1,j_2,k_1,k_2} = \exp(-d_{i_1,i_2,j_1,j_2,k_1,k_2}) \tag{8}$$

where $d_{i_1,i_2,j_1,j_2,k_1,k_2}$ can be considered as the similarity distance for the considered matching. This term is assumed to embed the properties related the underlying geometric structure (i.e. isoceles triangle). In this paper, focusing on a preliminary study, we only consider the difference between edges length of matched triangles:

$$d_{i_1,i_2,j_1,j_2,k_1,k_2} = |\mu_m(i_1,j_1) - \mu_r(i_2,j_2)| \\ + |\mu_m(i_1,k_1) - \mu_r(i_2,k_2)| + |\mu_m(j_1,k_1) - \mu_r(j_2,k_2)| \tag{9}$$

The final matching X^* is the matching $X \in P$ maximizing the score S:

$$X^* = \underset{X \in P}{\operatorname{argmax}}(S(X)) \tag{10}$$

Note that, due to the symmetry of the triangle, both identified eyes can be flipped by the matching, with respect to the model. In our case, this is managed by comparing their relative position, at head boundaries, with respect to the barycenter of the piglet head.

2.5 Brain segmentation

This step corresponds to Figure 1-D, where a 3D deformable model is used to retrieve brain boundaries. A key aspect of this step concerns the initialization of the 3D deformable model by a sphere automatically placed at the center of the brain. We consider the 2D coordinate system $(O,\vec{i},\vec{j})$ related to the triangle: the center O is the center of mass of the triangle and the two orthonormal vectors are associated to two orthogonal planes the intersection of which corresponding to the line passing through O and the barycenter of the nose (see Figure 1-D). The first plane is coplanar with the triangle. The second one is therefore perpendicular to the triangle. The estimated brain center B is defined, relatively to O by:

$$\overrightarrow{OB} = B_x\vec{i} + B_y\vec{j} \tag{11}$$

where B_x and B_y are assumed to be anatomical constants.

3 Experiments

Preliminary experiments aim at evaluating the relevance of this approach, focusing on the retrieval of the brain center from the initial image, as well as on the accuracy of the final brain extraction. One proposes to first study the relevance and the efficiency of the hypergraph matching step, based on the model graph that is assumed to be stable over piglets (anatomical invariant regarding distances between eyes and nose). One also

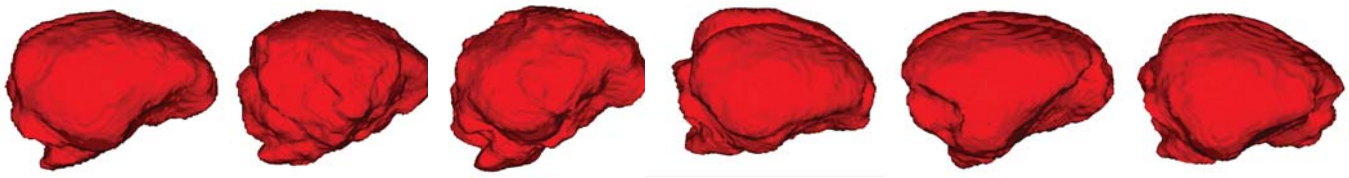

Figure 3. 3D models of automatically extracted piglet brains.

verifies that the position of the brain center with respect to the triangle is stable, to ensure an acceptable initialization of the deformable model. Finally, one evaluates the accuracy the resulting brain extraction.

3.1 Database

These preliminary experiments have been performed on a set of 6 3D MRI images, corresponding to 6 different piglets (2 weeks old piglets). For evaluation purposes, the coordinates of the barycenter of each eyes and of the nose have been manually estimated. This enabled to compute the model $G_{S,m}$ (mean relative distances). One also manually captured the coordinates of a reference point within the brain (barycenter of both lateral ventricles), to be used for deformable model initialization. The brain has also been manually segmented, for evaluating the entire procedure.

3.2 Results

The proposed approach has been implemented using the Python language together with appropriate scientific packages, and the ITK-SNAP software for manually capturing reference coordinates. For the hypergraph matching step, the number of candidates has been reduced by keeping the seven largest ones, in order to reduce computation time. Hypergraph matching has been done by testing all possible cases (set P, in equation 6), without any optimization [14, 15] because the paper focuses on showing the relevance of this hypergraph-matching-based problem formulation rather that on optimizing its implementation.

The *a priori* $G_{S,m}$ model is reported in Table 1 ($\mu_{S,m}$ function, corresponding to distances). Note the weak standard deviation, underlying that spatial relationships seem to be stable over piglets. Although the property of symmetry is not exploited in this preliminary work for hypergraph matching, it appears that the hypothesis of facing an isoceles triangle is relevant (distances of both eyes with respect to the nose are strongly similar).

On this set of piglets, the hypergraph matching led to a perfect identification of both eyes and nose, compared to manually identified structures (see Figure 2).

Values of B_x and B_y have been measured to be respectively 3.6 mm and 48.5 mm, averaged over the experimental database. This relative position has been used to evaluate the accuracy of the estimation of the brain center (reference point): the location of this reference point has been computed using

Distance ($\mu_{S,m}$)	Mean (standard deviation)
(`Leye`, `Reye`)	47.4 (1.9)
(`Leye`, `Nose`)	83.3 (2.3)
(`Reye`, `Nose`)	83.8 (2.2)

Table 1. Spatial model $G_{S,m}$, computed for the 6 piglets of the experimental database (mean distance, in millimeters, and standard deviation).

these mean values, and has been compared to manually captured 3D coordinates. The mean error has been measured to be of 1.7 mm (ranging between 0.5 mm and 4.4 mm, with a standard deviation of 1.6 mm), which is negligible with respect to approximative brain size (about 50 mm wide, manually estimated on one image).

For each piglet, the sphere has then been placed at the estimated reference point, to initialize the deformable model to finally extract the brain (see resulting 3D brain models reported in Figure 3). Automatically extracted piglet brains have been compared to manually segmented ones using the similarity index. The mean similarity index has been measured to be of 0.85 (ranging between 0.8 and 0.9, with a standard deviation of 0.04). The quality of the result has also been visually controled.

Although these preliminary results are promising, additional experiments are required on a larger database (only 6 piglets are considered in this paper), to validate the proposed approach. Concerning the last step regarding entire brain segmentation using deformable models, parameters have been manually tuned to obtain visually acceptable brain surfaces. Experiments on a larger database will involve an automated optimization of these parameters, in order to objectively quantify the best reachable similarity index, maybe better than the one observed on this small database. The initial hypothesis of the anatomical invariance of the relative position between the nose and both eyes appears relevant with respect to our purpose of retrieving an acceptable estimate of the brain center (compared to an estimate based on the barycenter of the entire head). Moreover, observed variations of these relative positions appear low enough to achieve a correct hypergraph-matching-based detection of the nose and both eyes.

4 Conclusion

According to these preliminary experiments, the proposed approach appears to be promising, with the advantage of being based on *a priori* knowledge that is easy to acquire and to formulate. From a methodological point of view, this work also illustrates how the perception of the scene (i.e. qualitative high-level relationships: "brighter than" and "included in", "triangular structure") can be connected to low level image features (intensities and coordinates in our case) and algorithms (e.g. binary thresholding in our case).

The next step will concern the experimental evaluation of the entire processing line on a larger database. Our proposal is based on spatial relationships that may significantly vary with, for instance, the age of the piglet (distances between eyes and nose). To overcome this limitation, an improvement would concern the adptation of our proposal so that the score used for hypergraph matching does not depend on these distances. We plan to favor other aspects such as the symmetry of the triangle and the sphericity of eyes (score depending on both edges and nodes of the hypergraph).

The perspective of this work concerns the application of this approach to other animals and other anatomical regions.

References

[1] H. Gan, Q. Zhang, H. Zhang, Y. Chen, J. Lin, T. Kang, J. Zhang, F. A. Troy, and B. Wang, "Development of new population-averaged standard templates for spatial normalization and segmentation of MR images for postnatal piglet brains," *Magnetic Resonance Imaging*, vol. 32, no. 10, pp. 1396 – 1402, 2014.

[2] C. N. Devi, A. Chandrasekharan, S. V.K., and Z. C. Alex, "Automatic segmentation of infant brain MR images: With special reference to myelinated white matter," *Biocybernetics and Biomedical Engineering*, vol. 37, no. 1, pp. 143 – 158, 2017.

[3] A. Makropoulos, S. J. Counsell, and D. Rueckert, "A review on automatic fetal and neonatal brain MRI segmentation," *NeuroImage*, vol. 170, pp. 231 – 248, 2018.

[4] J. D. Nielsen, K. H. Madsen, O. Puonti, H. R. Siebner, C. Bauer, C. G. Madsen, G. B. Saturnino, and A. Thielscher, "Automatic skull segmentation from MR images for realistic volume conductor models of the head: Assessment of the state-of-the-art," *NeuroImage*, vol. 174, pp. 587 – 598, 2018.

[5] S. M. Smith, "Fast robust automated brain extraction," *Human Brain Mapping*, vol. 17, no. 3, pp. 143–155, 2002.

[6] J.-B. Fasquel and N. Delanoue, "A graph based image interpretation method using a priori qualitative inclusion and photometric relationships," *IEEE Transactions on Pattern Analysis and Machine Intelligence*, 2019.

[7] J.-B. Fasquel and N. Delanoue, "An approach for sequential image interpretation using a priori binary perceptual topological and photometric knowledge and k-means based segmentation," *Journal of the Optical Society of America A*, 2018.

[8] I. Bloch, "Fuzzy sets for image processing and understanding," *Fuzzy Sets and Systems*, vol. 281, pp. 280–291, 2015.

[9] J.-B. Fasquel, V. Agnus, J. Moreau, L. Soler, and J. Marescaux, "An interactive medical image segmentation system based on the optimal management of regions of interest using topological medical knowledge," *Computer Methods and Programs in Biomedicine*, vol. 82, pp. 216–230, 2006.

[10] A. Moreno, C. Takemura, O. Colliot, O. Camara, and I. Bloch, "Using anatomical knowledge expressed as fuzzy constraints to segment the heart in CT images," *Pattern Recognition*, vol. 41, no. 8, pp. 2525 – 2540, 2008.

[11] O. Colliot, O. Camara, and I. Bloch, "Integration of fuzzy spatial relations in deformable models - application to brain MRI segmentation," *Pattern Recognition*, vol. 39, pp. 1401–1414, 2006.

[12] O. Nempont, J. Atif, and I. Bloch, "A constraint propagation approach to structural model based image segmentation and recognition," *Information Sciences*, vol. 246, pp. 1–27, 2013.

[13] J. Bernal, K. Kushibar, D. S. Asfaw, S. Valverde, A. Oliver, R. Mart, and X. Lladó, "Deep convolutional neural networks for brain image analysis on magnetic resonance imaging: a review," *Artificial Intelligence in Medicine*, pp. 64–81, 2019.

[14] O. Duchenne, F. Bach, I. Kweon, and J. Ponce, "A tensor-based algorithm for high-order graph matching," *IEEE Transactions on Pattern Analysis and Machine Intelligence*, vol. 33, no. 12, pp. 2383–2395, 2011.

[15] J. Zhou, T. Wang, C. Lang, S. Feng, and Y. Jin, "A novel hypergraph matching algorithm based on tensor refining," *Journal of Visual Communication and Image Representation*, vol. 57, pp. 69 – 75, 2018.